# X-ray absorption spectroscopic studies on gold nanoparticles in mesoporous and microporous materials

**Deepak B. Akolekar,[a]* Garry Foran[b] and Suresh K. Bhargava[a]**

*[a]Catalysis and Advanced Materials Research Group, Department of Applied Chemistry, RMIT University, City Campus, Melbourne, Victoria 3001, Australia, and [b]Australian Synchrotron Research Program, c/o ANSTO, PMB 1, Menai, NSW 2234, Australia. E-mail: e04781@ems.rmit.edu.au*

Au $L_3$-edge X-ray absorption spectroscopic measurements were carried out over a series of mesoporous and microporous materials containing gold nanoparticles to investigate the effects of the host matrix and preparation methods on the properties of gold nanoparticles. The materials of structure type MCM-41, ZSM-5, SAPO-18 and LSX with varying framework composition containing low concentrations of gold nanoparticles were prepared and characterized. In these materials the size of the gold nanoparticles varied in the range $\sim$1 to 4 nm. A series of gold nanoparticles within different mesoporous and microporous materials have been investigated using X-ray absorption fine structure (XANES, EXAFS) and other techniques. Information such as atomic distances, bonding and neighbouring environment obtained from XAFS measurements was useful in elucidating the nature and structure of gold nanoparticles on these catalytic materials. The influence of the high-temperature (823, 1113, 1273 K) treatment on gold nanoparticles inside the mesoporous matrix was investigated using the XAFS technique. The XAFS and XANES results confirm various characteristics of gold nanoparticles in these materials suitable for catalysis, fabrication of nanodevices and other applications.

**Keywords: gold nanoparticles; mesoporous materials; MCM-41; microporous materials; ZSM-5; LSX; low silica faujasite; EXAFS; XANES; SAPO-18; surface properties; Au.**

## 1. Introduction

The X-ray absorption technique is an important and useful technique in obtaining valuable information on the local structure and electronic state of the atoms constituting the catalytic material, site symmetry, the number and kind of neighbor atoms and their distances *etc.* (Eisenberger & Kincaid, 1978; Koningsberger & Prins, 1988). Application of the XAFS technique for investigating nanoparticles-based materials has proved to be crucial in extracting structural information on various nanoparticles. Nanoparticles are new-generation advanced materials with unique properties (physical, magnetic, optical, surface structural properties) with potential in developing new technologies, techniques, improvement of old methods/processes in catalysis, sensor technology, and fabrication of nanodevices (Zhdanov & Kasemo, 2002; Gorodetskii & Drachsel, 1999; Kobayashi *et al.*, 1990). Gold exhibits a unique catalytic nature and action when it is deposited as nanoparticles on a variety of metal oxides. Gold nanoparticles supported on metal oxides have been shown to be highly active for the low-temperature oxidation of CO, complete oxidation of hydrocarbons and selective partial oxidation of propylene (Haruta, 1997*a*,*b*; Haruta *et al.*, 1987, 1989; Gupta & Tripathi, 1999). Gold catalysts are important in the areas of selective oxidation and hydrogenation of organics, and the dispersion of gold on the support material affects their catalytic ability. Interaction between deposited gold nanoparticles and the support has a significant effect on the catalytic properties and is highly sensitive to the structure of Au. Improved knowledge of the structure of gold nanoparticles and its interaction with the metal oxide support can lead to better designing of the gold catalysts. The adsorption and catalytic activity strongly depends on the composition, particle size, structure and support type as well as on the material structure (Walker *et al.*, 2001; Brust *et al.*, 1994; Uphade *et al.*, 2001; Haruta, 1997*a*,*b*).

Catalyst performance and economic viability are the important criteria for material selection and, over a number of years, research has focused on metal mesoporous [metal modified MCM-41 (Jeon *et al.*, 2003; Kresge *et al.*, 1992; Chen *et al.*, 1997)] and microporous [metal ZSM-5, metal SAPO-18 (Akolekar & Bhargava, 1998; Akolekar *et al.*, 1998; Wilson *et al.*, 1982)] commercial catalysts. MCM-41 is a synthetic mesoporous material with regular well defined channel systems, large surface area, low acidity and thermal stability. These material properties could be easily manipulated by varying the incorporation of aluminium or other elements into the framework. MCM-41 materials exhibit high activity for NO and CO conversions, $n$C$_{16}$ cracking and good selectivity for producing low carbon alkylenes, as well as for phenol methylation *etc.* (Chen *et al.*, 1997; Bhattacharyya *et al.*, 2003). The catalytic properties of the ZSM-5 and SAPO-18 materials largely depend upon the Si/Al ratio, degree of cation exchange, extra-framework element, surface treatment *etc*. Inclusion of active nanometal particles such as gold nanoparticles enhances the catalytic properties of these materials.

The present study was undertaken in order to characterize gold catalysts (prepared by different methods and support matrix structures) using XAS. The synthesis of highly dispersed gold particles is highly sensitive to preparation conditions and support material; so far, no systematic XAS studies have been reported (Kobayashi *et al.*, 1990; Haruta *et al.*, 1987). This paper deals with the application of X-ray absorption fine structure (XAFS) for investigating the gold nanoparticles in different support matrix structures prepared by different methods, using different gold concentrations and high-temperature treatments so that the XAS can be employed for preparation of catalysts with definitive gold properties. The gold catalysts prepared by different methods and using different supports (MCM-41, ZSM-5, LSX, SAPO-18) were investigated using XAFS and other instrumental techniques. The advantage of using microporous and mesoporous materials for gold nanoparticles inclusion is that the metal particle size can be contained at certain levels during catalytic treatments and usage at higher temperatures.

## 2. Experimental section

Mesoporous (MCM-41) and microporous (ZSM-5/LSX) materials containing gold nanoparticles were prepared using hydrothermal crystallization methods (Bellussi *et al.*, 1988; Ryoo *et al.*, 1996; Akolekar & Bhargava, 2004; Akolekar, 1993; Akolekar *et al.*, 1997; Kladis *et al.*, 2000). The preparations of MCM-41, ZSM-5 and LSX are well known. During preparation of the synthetic gel mixture (MCM-41/ZSM-5/LSX) an appropriate amount of dilute gold compound ($HAuCl_4$) solution was added very slowly and continuously at 315 K for a period of 5 h under an inert atmosphere. The synthetic mixture was hydrothermally crystallized at 368 K for MCM-41 (crystallization period 75 h), 433 K for ZSM-5 (120 h) and 348 K for LSX (144 h). After the completion of crystallization, the material was thoroughly washed with de-ionized water and heated at

  DOI: 10.1107/S0909049504001694 

353 K for 16 h and further at 773 K for 8 h. A detailed description of the preparation of gold nanoparticles material is given elsewhere (Akolekar & Bhargava, 2004; Tsubota *et al.*, 1991). The chemicals used in the synthesis of the materials were Catapal (aluminium oxyhydroxide), *o*-phosphoric acid (85%, Merck), Aerosil (fumed silica), Ludox HS-40 (Aldrich), tetrapropylammonium hydroxide (Aldrich), cetyl trimethyl ammonium chloride (CTACl) solution (Aldrich), sodium hydroxide (BDH), *N*,*N*-diisopropylethylamine (99%, Aldrich) and water-based gold chloride solution.

For the purpose of comparison, certain gold-particle-containing materials were also prepared by using the deposition–precipitation method (Tsubota *et al.*, 1991). The gold-containing materials were prepared by immersing the calcined material (ZSM-5/SAPO-18/MCM-41) in dilute $HAuCl_4$ ($<0.4$ g $L^{-1}$) solution at 328 K for 7 h (pH $\sim$6.4) with continuous stirring. The precursor was washed, dried and calcined at 643 K for 5 h. During the sample preparation, the gold precursor was deposited into the pores of material and precipitated as $Au(OH)_2$, and, with further heating of the sample at 643 K, $Au(OH)_2$ was reduced to metallic gold [Au(0)] (Tsubota *et al.*, 1991). The high-purity SAPO-18 (Kladis *et al.*, 2000), ZSM-5 and MCM-41 materials were used for preparing the gold materials. For studying the influence of high temperatures (>823 K) on the properties of gold nanoparticles, the as-prepared Au MCM-41 (*a*) (Table 1) sample was heated at different temperatures (473, 823, 1123 and 1273 K) in an inert (helium) atmosphere. The materials were characterized for their chemical composition, phase purity, structure, surface properties and particle size using standard and sophisticated instrumental techniques such as ICP-MS (HP4500 Series 300), XRD (Bruker D8 Advance), BET, TEM (Jeol 1010 at 100 kV) *etc.*, respectively. The surface area and micropore and total pore volume of the materials were obtained by $N_2$ dynamic adsorption/desorption techniques ($p/p_0 = 0.3$) using a Micromeritics ASAP2000 Instrument. Details of the instruments utilized and characterization methods are reported elsewhere (Akolekar *et al.*, 1998; Akolekar, 1993).

Au $L_3$-edge EXAFS spectra were recorded in fluorescence mode at the Australian National Beamline Facility (ANBF), beamline 20B (bending magnet) at the 2.5 GeV Photon Factory (KEK, Tsukuba, Japan). The excitation energy was selected using a water-cooled Si(111) channel-cut crystal monochromator (11 m from the light source). The beam size of 2 mm (horizontal) $\times$ 1 mm (vertical) was controlled using a slit assembly (13 m from the source). Energy calibration was performed by using an Au foil as an internal standard and from time to time the energy reproducibility was checked. Fluorescence was measured using a Canberra GL0110S ten-element Ge array detector. The signal from each array element was passed from the detector, *via* a Canberra Model 2026XA spectroscopy amplifier (shaping time 0.25 µs), to a Canberra Model 2030 single-channel analyzer, which was set to pass the Au $L_3$-edge signal to the counting electronics. For all samples, four/six scans (scan time $\sim$60 min) were taken in the energy range 11800–12800 eV. The fluorescence was normalized to the incident beam flux monitored by an ionization chamber with a path length of 30 cm.

The spectra were recorded (in fluorescence mode) at room temperature. Powder samples were pressed into (<0.5 mm-thick) pellets supported in an aluminium spacer between Kapton tape windows. The spectra were averaged from four to five scans. Averaging, background subtraction, random errors (arising due to noise) and calculation of theoretical EXAFS spectra were performed using the *XFIT* software package (XFIT, 1995). The model fitting calculations were performed using the *XFIT* program, where a non-linear least-squares procedure was used to fit the model parameters to the observed XAFS (Ellis & Freeman, 1995; XFIT, 1995). *XFIT* incorporates *ab initio* calculations of the XAFS using the programs *FEFF*4.06 for single scattering and *FEFF*6.01 for multiple scattering (XFIT, 1995). The parameters, such as coordinates of all atoms, Debye–Waller factors, threshold energy *etc.*, were varied to optimize the agreement between the calculated and observed XAFS. The observed and calculated XAFS were Fourier-filtered and the goodness-of-fit parameter and statistical errors were estimated according to the reported methods (Ellis & Freeman, 1995). The entire $\chi$ function was fit; however, for clarity in certain figures only a magnitude of data is presented. For EXAFS measurements, 13 samples were selected which included as-prepared (Au ZSM-5 and Au MCM-41 with different Au, Si and Al concentrations), gold deposited–precipitated (SAPO-18, ZSM-5, AlMCM-41) and heated-treated (Au MCM-41 at 473 K, 823 K, 1113 K and 1273 K) samples.

**Table 1**
Chemical composition of gold-nanoparticles-containing mesoporous and microporous materials.

| Material type | Product composition (mol %) | | | | Si/Au | Si/Al |
|---|---|---|---|---|---|---|
| | Au | Al | Si | P | | |
| MCM-41 | | 2.91 | 97.09 | | | 33.36 |
| Au MCM-41 (*a*) | 2.02 | 2.90 | 95.08 | | 47 | 32.78 |
| Au MCM-41 (*b*) | 0.386 | 2.92 | 96.694 | | 250 | 33.11 |
| ZSM-5 | | 2.16 | 97.84 | | | 45.29 |
| Au ZSM-5 (*c*) | 0.166 | 2.434 | 97.4 | | 586 | 40.01 |
| Au ZSM-5 (*d*) | 0.99 | 2.063 | 96.947 | | 97.92 | 46.99 |
| Au ZSM-5 (*e*) | 1.161 | 1.498 | 97.341 | | 83.84 | 64.98 |
| Au LSX (*f*) | 0.646 | 48.60 | 50.754 | | 78.56 | 1.044 |
| Au SAPO-18(*g*)† | 0.14 | 46.30 | 8.88 | 44.68 | 63.42 | 0.191 |
| Au ZSM-5 (*h*)† | 1.09 | 2.21 | 96.70 | | 88.71 | 43.75 |
| Au MCM-41 (*i*)† | 1.312 | 2.877 | 95.811 | | 73.02 | 33.30 |

† Deposition–precipitation method.

## 3. Results and discussion

Mesoporous (MCM-41) and microporous (ZSM-5, LSX, SAPO) materials are normally used as catalyst or support owing to their high surface area. The high-purity mesoporous (MCM-41 type) and microporous [high-silica pentasil zeolite (ZSM-5), low-silica faujasite (LSX) and silicoaluminophosphate (SAPO-18)] materials containing various loadings of gold nanoparticles were prepared. These materials were chosen because they provide a high surface area, different microporous or mesoporous structure and may act as active co-catalyst or inert support material. The gold nanoparticles-containing materials and their chemical composition are given in Table 1. Chemical analysis of the samples showed that the concentration of gold varied (range 1–4 wt% Au) with the host structures [mesoporous (MCM-41) and microporous (ZSM-5, LSX and SAPO-18)]. The XRD analysis confirmed the desired structure and phase purity of the MCM-41, ZSM-5, LSX and SAPO-18 samples and the presence of gold (f.c.c.) in these materials.

Investigation of the surface characteristics (surface area, pore volume, adsorption/desorption isotherm, pore size and volume distribution) of the gold-containing samples (Table 2) suggested their well defined mesoporous/microporous nature. The pure MCM-41, ZSM-5, LSX and SAPO-18 samples exhibited slightly higher surface area, micropore and total pore volume as compared with gold-containing microporous and mesoporous samples. The decrease in the surface area and pore volumes is expected owing to occupation of pore space by gold particles. In these gold nanoparticles materials, decrease in the surface area, micropore and total pore volume is

**Table 2**
Particle size and surface characteristics of the gold-nanoparticles-containing mesoporous and microporous materials.

| Material type | Gold particle size (on as-prepared samples) (nm) | Surface properties | | |
|---|---|---|---|---|
| | | Surface area ($m^2\ g^{-1}$) | Micropore volume ($cm^3\ g^{-1}$) | Total pore volume ($cm^3\ g^{-1}$) |
| MCM-41 | | 1315 | 0.013 | 1.40 |
| Au MCM-41 (*a*) | 3–4 | 1270 | 0.005 | 1.35 |
| Au MCM-41 (*b*) | ~2 | 930 | 0.01 | 0.935 |
| ZSM-5 | | 575 | 0.24 | 0.31 |
| Au ZSM-5 (*c*) | ~1 | 473 | 0.165 | 0.185 |
| Au ZSM-5 (*d*) | 2–3 | 513 | 0.20 | 0.24 |
| Au ZSM-5 (*e*) | ~1–2 | 548 | 0.22 | 0.29 |
| Au LSX (*f*) | ~2 | 359 | 0.155 | 0.17 |
| Au SAPO-18 | 2–3 | 424 | 0.135 | 0.14 |
| Au ZSM-5 (*h*) | 2–2.5 | 364 | 0.13 | 0.155 |
| Au MCM-41 (*i*) | 2–3 | 850 | 0.006 | 0.84 |
| Au MCM-41 (*a*)† | >5 | 1235 | 0.00485 | 1.34 |

† Temperature 1113 K.

observed with an increase in the gold loading. TEM analysis of the gold-loaded materials showed the presence of gold in nanoparticulate form, with average nanoparticle size ranging between ~1 and 5 nm (varying from sample to sample), and the high-temperature treatments reflected the increase in the gold particle size. Details of the gold nanoparticle size are presented in Table 2.

EXAFS data were obtained for gold nanoparticles on the different mesoporous (>900 $m^2\ g^{-1}$) and microporous (>359 $m^2\ g^{-1}$) materials at room temperature using the ANBF's experimental set-up. The gold nanoparticles on various material structures [as-synthesized: Au MCM-41 (*a*) (Si/Au 47.1), Au MCM-41 (*b*) (Si/Au 250), Au ZSM-5 (*c*) (Si/Au 587), Au ZSM-5 (*d*) (Si/Au 98), Au ZSM-5 (*e*) (Si/Au 83.9), Au LSX (*f*) (Si/Au 78.6); thermally treated: Au MCM-41 (*a*) at 473, 823, 1113, 1273 K; gold deposited-precipitated: SAPO-18, ZSM-5 (*h*), MCM-41 (*i*)] were investigated for Au $L_3$ XAFS in order to elucidate variations in the local environment and structure around the gold atom. X-ray absorption spectra of gold nanoparticles on different matrices of types such as MCM-41, ZSM-5 and LSX [containing low loadings of gold nanoparticles (Table 1)] materials exhibit slight differences in the peak height and fineness in features, with the difference being more prominent in Au LSX. The XAFS spectra (Au $L_3$-edge) of these materials were moreover similar to that of metallic gold (Guillemot *et al.*, 1999).

Figs. 1 and 2 show the experimental (solid black lines) and theoretical (calculated best fits; dotted lines) plots of the Au $L_3$-edge $k$-weighted EXAFS function $k\chi(k)$ and Fourier transform of as-prepared Au MCM-41/ZSM-5/LSX samples. The differences between the experimental and theoretical curves are shown as residual curves in the figures. For all the samples, the goodness-of-fit value ($R$) was in the range 20–25% (Tables 3 and 4) and the value of the energy $E$ in the fitting procedure varied from −4 to −9 eV. The XAFS (Fig. 1) and Fourier transforms (Fig. 2) show the presence of a few oxidic gold species (Au—O) with majority of metallic gold species (Au—Au). The similarity of XANES and Fourier transforms in various structures (MCM-41, ZSM-5, LSX) with different gold concentration indicates that the local structure around the gold atom is very similar despite the material structure. However, in the case of the Au LSX, the signals observed between 1.2 and 2.0 Å are more prominent than for the other Au materials. On the radial distribution curve, the characteristic profile of metallic gold is easily recognized (Au—Au ~2.72 ± 0.02 Å). A signal at about 1.6 to 1.8 Å observed in the radial distribution curve is characteristic of oxidized gold

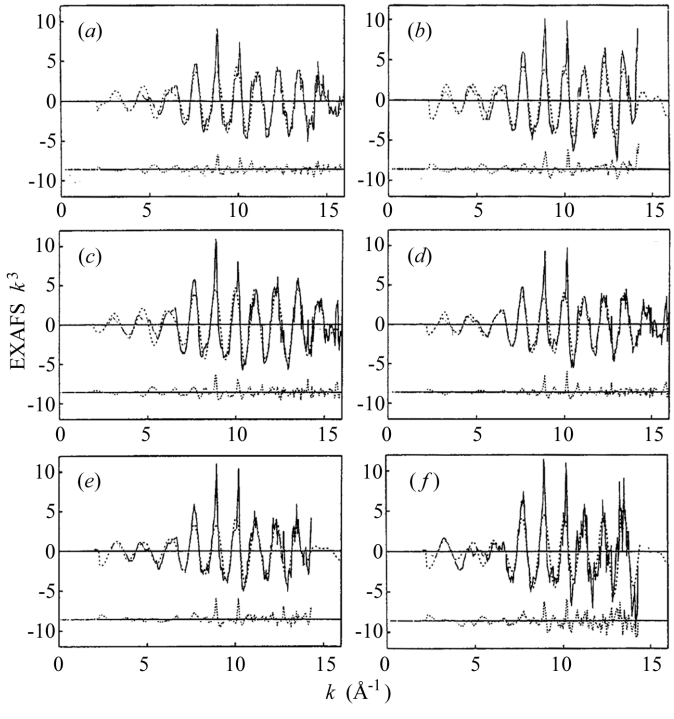


**Figure 1**
EXAFS spectra (Au $L_3$) of gold nanoparticles on different mesoporous and microporous materials [as-prepared: (*a*) Au MCM-41 (*a*); (*b*) Au MCM-41 (*b*); (*c*) Au ZSM-5 (*c*); (*d*) Au ZSM-5 (*d*); (*e*) Au ZSM-5 (*e*); (*f*) Au LSX (*f*)]. The solid lines are experimental data and the overlaid dotted lines are best fits (calculated). The lower curve in each shows the residuals.

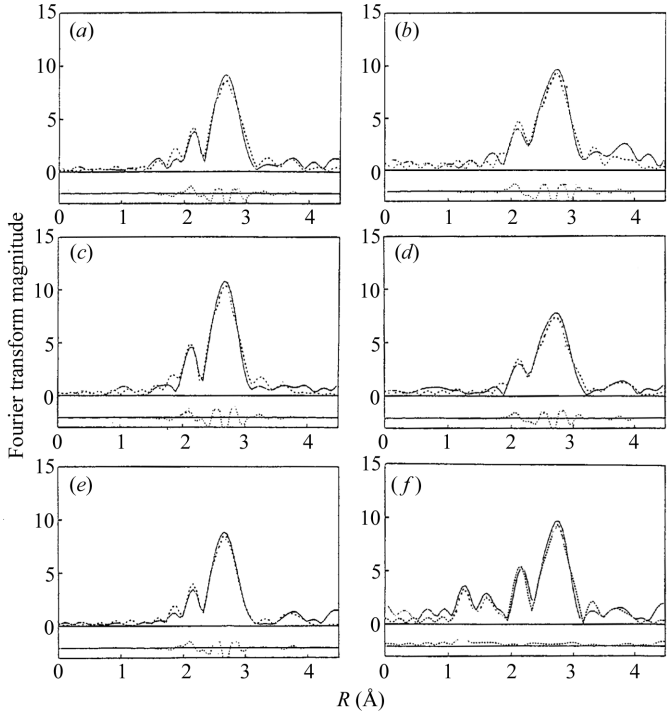


**Figure 2**
EXAFS Fourier transforms (Au $L_3$) of gold nanoparticles on different mesoporous and microporous materials [as-prepared: (*a*) Au MCM-41 (*a*); (*b*) Au MCM-41 (*b*); (*c*) Au ZSM-5 (*c*); (*d*) Au ZSM-5 (*d*); (*e*) Au ZSM-5 (*e*); (*f*) Au LSX (*f*)]. The solid lines are experimental data and the overlaid dotted lines are best fits (calculated). The lower curve in each shows the residuals.

**Table 3**
Atomic distances, Debye–Waller factor and *R* factor of gold nanoparticles in as-prepared mesoporous and microporous materials.

M = O/Cl/N. $A_i$ = Debye–Waller factor of the *i*th shell.

| Material type | Atom type | Bond length (Å) | $A_i$ (Å$^2$) | *R* factor (%) | Symmetry |
|---|---|---|---|---|---|
| Au MCM-41 (*a*) | O | 1.6 | 0.0034 (1) | 22.21 | f.c.c. |
| | O | 1.9 | 0.004 (1) | | |
| | Cl | 2.15 | 0.003 (2) | | |
| | Au | 2.71 | 0.0055 (1) | | |
| Au MCM-41 (*b*) | O | 1.72 | 0.0049 (1) | 24.7 | f.c.c. |
| | Cl | 2.12 | 0.0044 (1) | | |
| | Au | 2.76 | 0.006 (2) | | |
| Au ZSM-5 (*c*) | O | 1.68 | 0.0030 (2) | 23.8 | f.c.c. |
| | Cl | 2.13 | 0.004 (1) | | |
| | Au | 2.70 | 0.005 (2) | | |
| Au ZSM-5 (*d*) | O | 1.70 | 0.00460 (1) | 26.5 | f.c.c. |
| | Cl | 2.20 | 0.002 (1) | | |
| | Au | 2.74 | 0.007 (2) | | |
| Au ZSM-5 (*e*) | O | 1.80 | 0.0018 (2) | 25.04 | f.c.c. |
| | Cl | 2.18 | 0.003 (1) | | |
| | Au | 2.70 | 0.004 (1) | | |
| Au LSX (*f*) | O | 1.62 | 0.0047 (1) | 26.5 | f.c.c. |
| | Cl | 2.20 | 0.0033 (1) | | |
| | Au | 2.70 | 0.0081 (2) | | |

**Table 4**
Atomic distances, Debye–Waller factor and *R* factor of the high-temperature treated gold nanoparticles materials and Au deposited–precipitated microporous and mesoporous materials.

M = Au/O/Cl/metal. $A_i$ = Debye–Waller factor of the *i*th shell.

| Material type | Atom type | Bond length (Å) | $A_i$ (Å$^2$) | *R* factor (%) | Symmetry |
|---|---|---|---|---|---|
| Au MCM-41 (*a*) (473 K) | O | 1.85 | 0.003 (1) | 26.9 | f.c.c. |
| | Cl | 2.18 | 0.004 (1) | | |
| | Au | 2.74 | 0.0049 (2) | | |
| Au MCM-41 (*a*) (823 K) | O | 1.9 | 0.011 (1) | 23.3 | f.c.c. |
| | O | 2.18 | 0.004 (3) | | |
| | Au | 2.74 | 0.0069 (2) | | |
| Au MCM-41 (*a*) (1113 K) | Au/O | 2.14 | 0.0040 (1) | 27.1 | f.c.c. |
| | Au | 2.77 | 0.008(1) | | |
| Au MCM-41 (*a*) (1273 K) | Au/O | 2.13 | 0.002 (2) | 23.5 | f.c.c. |
| | Au | 2.79 | 0.0092 (1) | | |
| Au SAPO-18 | O | 1.65 | 0.0018 (2) | 26.7 | f.c.c. |
| | O | 2.25 | 0.004 (1) | | |
| | Au | 2.72 | 0.0059 (2) | | |
| Au ZSM-5 (*h*) | O | 1.72 | 0.0043 (1) | 26.8 | f.c.c. |
| | O | 2.16 | 0.005 (1) | | |
| | Au | 2.73 | 0.006 (2) | | |
| Au MCM-41 (*i*) | O | 1.80 | 0.0044 (1) | 27.2 | f.c.c. |
| | O | 2.15 | 0.003 (1) | | |
| | Au | 2.73 | 0.003 (2) | | |

surrounded by light atoms (mostly short Au—O bonds). The bond length and other parameters (Debye–Waller factor and *R* factor) results obtained from EXAFS analysis are summarized in Table 3. Kageyama *et al.* (1993) have assigned the signal at around 2.2 ± 0.2 Å (the short Au—Au bond) to binding of Au with the Au or support elements or Cl (designated as M). The Au materials mostly show three to four types of different coordination number. When small gold clusters are examined by the EXAFS method, the apparent average coordination number is smaller than that observed in the bulk metal because of the high proportion of surface atoms. This effect is dependent on the size and shape of the metal cluster (Greegor & Lytle, 1980). The magnitude of the Au—Au and Au—M peaks as well as their relative ratios in the radial distribution function slightly varied in different host (mesoporous and microporous) matrices. The presence of small gold particles is clearly indicated by the observed low Au—Au signal at ∼2.72 ± 0.02 Å. These results are in agreement with the reported ones (Guillemot *et al.*, 1999; Kageyama *et al.*, 1993). The observed Au—Au in the gold foil is ∼2.85 Å. The XRD measurements on the gold nanoparticles in the mesoporous and microporous materials indicated a face-centered cube structure. XAFS identified the presence of Au—O (∼0.16 nm) (coordination number >1), Au—O (∼0.19 nm) (∼3), Au—M (M = Au/Cl/support element) (∼0.22 nm) (2–3) and Au—Au (>0.276 nm) (>4) in the various different host support structures. The possible single- and multiple-scattering paths (Rich *et al.*, 1998) contributing to the XAFS in a gold nanoparticles material (Au/O, M = Au/Cl/support elements) system are as follows:

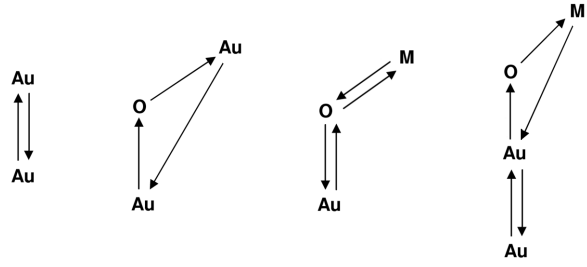


The high-temperature (above 823, 1113, 1273 K) treated Au MCM-41 (*a*) samples showed minor changes in the peak height and features of the XAFS spectra. BET analysis of the thermally treated Au MCM-41 (*a*) sample at 1113 K exhibited only slight reduction (∼3%) in surface area, micro and total pore volume. The Au $L_3$-edge *k*-weighted EXAFS function $k\chi(k)$ along with best-fit (*R* factors in the range 22–26%) and corresponding radial distribution curves of as-prepared and thermally treated Au MCM-41 (*a*) samples are shown in Figs. 3 and 4. The magnitude of Au—O, Au—M and Au—Au and their ratios are not significantly affected up to the temperature of 823 K. However, the high-temperature treatments given to the gold nanoparticles material [Au MCM-41 (*a*)] (at 1113 and 1273 K) showed significant changes in the magnitude of Au—O, Au—M and Au—Au and their ratios (Fig. 4) and peak width. In the case of the samples treated above 1113 K, observation of no peak related to the oxidic gold species indicated the transformation of oxidic gold species to Au—Au. Table 4 shows the atomic distances, Debye–Waller factor and *R* factor parameters in the thermally treated Au MCM-41 material at 473, 823, 1113 and 1273 K. The changes in bond lengths of Au were observed due to the thermal treatments at 1113 and 1273 K. TEM measurement showed that the gold particle size increased up to certain levels with the treatment temperature (above 823 K). The increase in particle size is due to gold particle aggregation. It seems that micropores (in the host matrix) and uniform dispersion of gold particles are responsible for the limited increase in the particle size. Kageyama *et al.* (1993) explained the observed low Au—Au occupancy numbers (4 and 7) at 0.275 nm between 523–553 K on the basis of small gold particle size with >13 atoms.

EXAFS and Fourier transforms (Au $L_3$) of gold nanoparticles [Au SAPO-18 (*g*), Au ZSM-5 (*h*) and Au MCM-41 (*i*)] materials prepared by the deposition–precipitation method are presented in Fig. 5. The bond lengths, Debye–Waller factor and *R* factor of Au are summarized in Table 4. In the Au SAPO-18 (*g*), Au ZSM-5 (*h*) and Au MCM-41 (*i*) samples, variation in the bond lengths of Au—O, Au—M and Au—Au were observed. In these Au deposited–precipitated materials the magnitude of Au—O, Au—M and Au—Au and their ratios are different (Fig. 5), though these materials were prepared in a similar way, and with nearly similar Si/Au ratios.

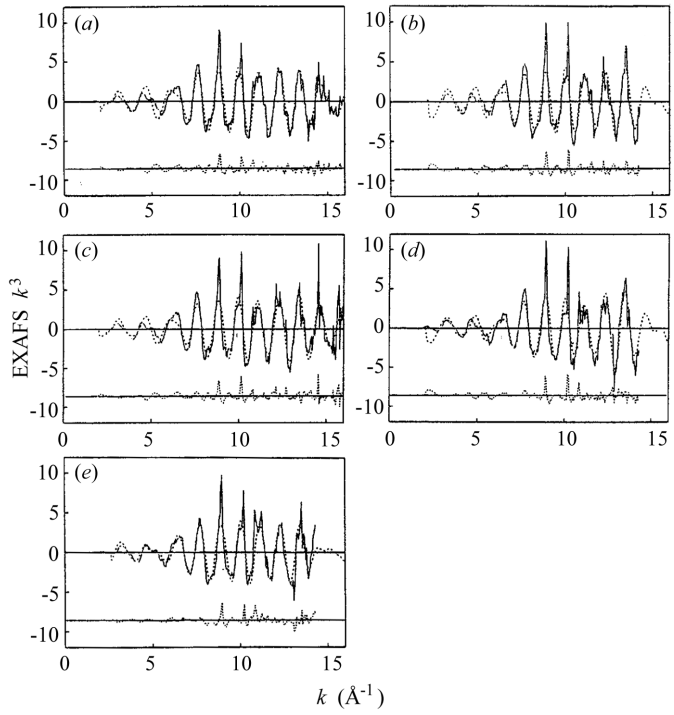


**Figure 3**
EXAFS spectra (Au $L_3$) of gold nanoparticles on mesoporous materials [as-prepared: (*a*) Au MCM-41 (*a*); (*b*) Au MCM-41 (*a*) (heat treated at 473 K, 3 h); (*c*) Au MCM-41 (*a*) (heat treated at 823 K, 3 h); (*d*) Au MCM-41 (*a*) (heat treated at 1113 K, 3 h); (*e*) Au MCM-41 (*a*) (heat treated at 1273 K, 3 h)]. The solid lines are experimental data and the overlaid dotted lines are best fits (calculated). The lower curve in each shows the residuals.

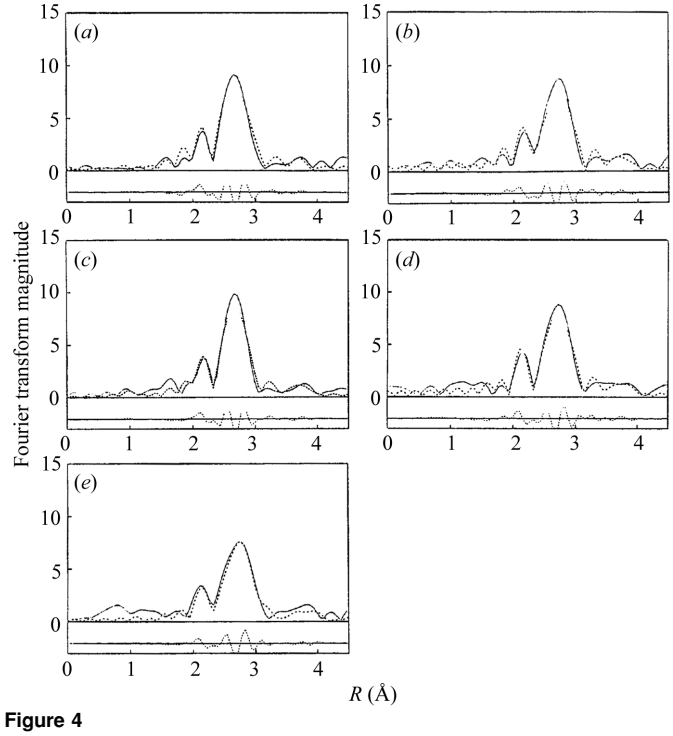


**Figure 4**
EXAFS Fourier transforms (Au $L_3$) of gold nanoparticles on mesoporous materials [as-prepared: (*a*) Au MCM-41 (*a*); (*b*) Au MCM-41 (*a*) (heat treated at 473 K, 3 h); (*c*) Au MCM-41 (*a*) (heat treated at 823 K, 3 h); (*d*) Au MCM-41 (*a*) (heat treated at 1113 K, 3 h); (*e*) Au MCM-41 (*a*) (heat treated at 1273 K, 3 h)]. The solid lines are experimental data and the overlaid dotted lines are best fits (calculated). The lower curve in each shows the residuals.

The XANES provide information about the site symmetry, spin state, atomic position of neighbours (interatomic distances and bond angles) and oxidation state of the metal. The edge shift (binding-energy shift) of the element is related to the oxidation state. The exact quantitative derivation of structural information from XANES is difficult (Kageyama *et al.*, 1993). Figs. 6–8 show the XANES Au $L_3$-edge spectra of gold nanoparticles on different as-synthesized mesoporous and microporous materials, thermally treated mesoporous material and gold deposited–precipitated materials, respectively. The XANES spectra were background corrected. The XANES shows significant variations for the gold nanoparticles prepared under different synthesis conditions, using different support materials and treatments. The XANES clearly indicates the presence of oxidized as well as reduced Au species. Figs. 6–8 show four distinct edge features; the 'white line' peak (~11 928 eV) is suppressed in all of the XANES spectra owing to the full occupancy of *d* states for gold. The other peaks after ~11 940 eV represent resonance features characteristics of the extended local structure around the absorbing atom (Benfield *et al.*, 2001). The peak around 11 940 eV is a weak feature but mostly present in bulk gold, gold nanoparticles *etc.* The two peaks between 11 940 and 11 980 eV (in the higher-energy part of the XANES) are more structure dependent.

It is interesting to note that the XANES spectrum (Fig. 7) for gold nanoparticles present in different host structures is different. The peaks in the 11 925 to 11 980 eV regions suggest that factors such as concentration of gold nanoparticles, host structure and host framework composition influences the XANES. Similarly, in the case of materials thermally treated (473, 823, 1273 K) on gold nanoparticles [Au MCM-41 (*a*)], shifts in the peaks of XANES spectra (Fig. 7) are observed in the higher-energy region of XANES. In gold deposited–precipitated materials (Fig. 8), Au SAPO-18 (*g*) exhibits different XANES patterns than Au ZSM-5 (*h*) and Au MCM-41 (*i*) materials.

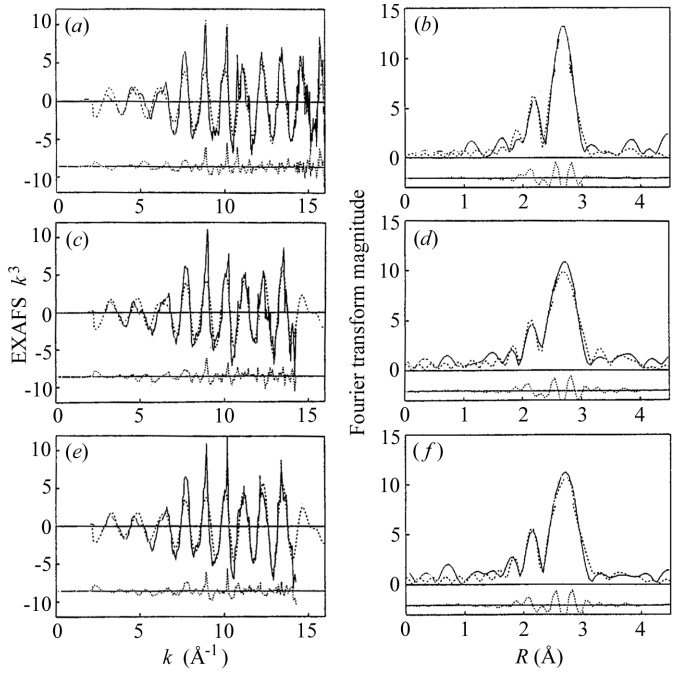


**Figure 5**
EXAFS and Fourier transforms (Au $L_3$) of gold nanoparticles (deposited–precipitated) on different microporous and mesoporous materials [(*a*)–(*b*) Au SAPO-18 (*g*); (*c*)–(*d*) Au ZSM-5 (*h*); (*e*)–(*f*) Au MCM-41 (*i*)]. The solid lines are experimental data and the overlaid dotted lines are best fits (calculated). The lower curve in each shows the residuals.

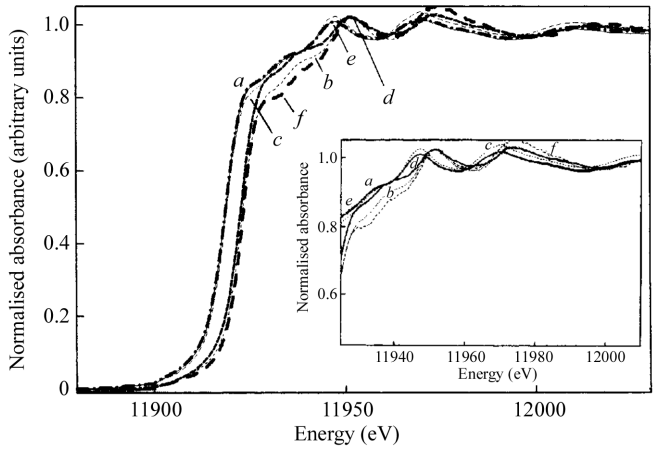


**Figure 6**
Au $L_3$-edge XANES spectra of gold nanoparticles on different mesoporous and microporous materials [as-prepared: (*a*) Au MCM-41 (*a*); (*b*) Au MCM-41 (*b*); (*c*) Au ZSM-5 (*c*); (*d*) Au ZSM-5 (*d*); (*e*) Au ZSM-5 (*e*); (*f*) Au LSX (*f*)].

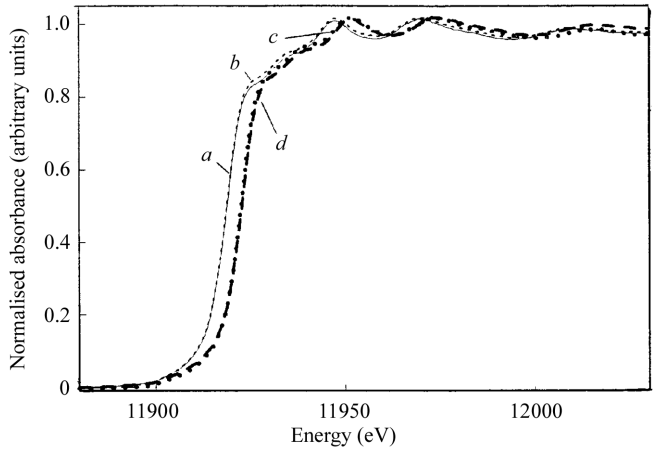


**Figure 7**
Au $L_3$-edge XANES spectra of gold nanoparticles on mesoporous materials [as-prepared: (*a*) as prepared Au MCM-41 (*a*); (*b*) Au MCM-41 (*a*) (heat treated at 823 K, 3 h); (*c*) Au MCM-41 (*a*) (heat treated at 1113 K, 3 h); (*d*) Au MCM-41 (*a*) (heat treated at 1273 K, 3 h)].

The XANES pattern of Au MCM-41 (*i*) is different than that of as-prepared Au MCM-41 (*a*). The intensity and width of these XANES peaks can be related to the number of neighbours surrounding each gold atom as well as to the size of the gold particle (Greaves *et al.*, 1981; Bazin *et al.*, 1997). In XANES spectra (Figs. 6–8), the intense and defined peaks (in the higher XANES region) are consistent with the reported results on gold nanoparticles (Benfield *et al.*, 2001). The XAS and XANES results are in agreement with the previously reported results.

## 4. Conclusions

The XANES and Fourier transform show the presence of a few oxidic gold species with the majority of them being metallic gold species (either Au—Au or Au—Me) on the Au MCM-41, Au ZSM-5, Au LSX and Au deposited–precipitated materials and high-temperature treated Au MCM-41 samples. In these samples the magnitude of Au—O/Au—Au in the radial distribution function is affected. XAFS

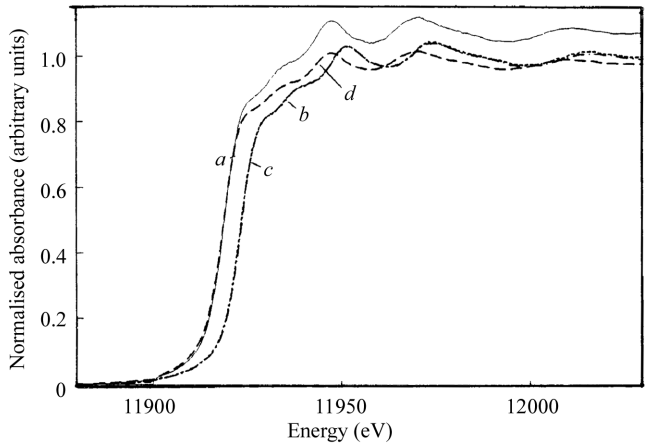


**Figure 8**
Au $L_3$-edge XANES spectra of gold nanoparticles (deposited–precipitated) on different microporous and mesoporous materials [(*a*) Au SAPO-18; (*b*) Au ZSM-5 (*h*); (*c*) Au MCM-41 (*i*)], (*d*) as-prepared Au MCM-41 (*a*)].

identified the presence of Au with different bond lengths in the various different host support structures. The presence of small gold nanoparticles is clearly indicated by the observed low Au—Au signal at $\sim 2.72 \pm 0.02$ Å. The mesoporous and microporous support influences various characteristics of gold nanoparticles. The TEM results indicate that the dispersion and size of gold nanoparticles are different in the materials with MCM-41, ZSM-5, SAPO-18 and LSX structures. The high-temperature treatments (>1113 K in particular) to gold nanoparticles significantly affect the magnitude of Au—O, Au—M/Au—Au, their ratios and the transformation of oxidic gold species to Au—M or Au—Au. The XAFS results show that the host matrix structure, metal concentration, size, dispersion and the thermal treatments influence the properties of gold nanoparticles. XAS study clearly indicates the difference between the gold nanoparticles prepared by different methods such as metal deposition–precipitation and hydrothermal synthesis. The XANES show striking and apparently consistent variations in the Au edge under the different sample preparation and treatment conditions.

We gratefully acknowledge the financial support of the Australian Synchrotron Research Program (Australian Nuclear Science and Technology Organization, ANSTO), Sydney. We thank the ANBF (Australian National Beamline Facility, 20B) team, Photon Factory of the National Laboratory for High Energy Physics (KEK), Tsukuba, Japan, for assistance and facility support. This work was performed at the Australian National Beamline Facility with support from the Australian Synchrotron Research Program, which is funded by the Commonwealth of Australia under the Major National Research Facilities Program.

## References

Akolekar, D. B. (1993). *J. Catal.* **143**, 227–238.
Akolekar, D. B. & Bhargava, S. K. (1998). *Stud. Surf. Sci. Catal.* **105**, 755–761.
Akolekar, D. B. & Bhargava, S. K. (2004). *Appl. Catal.* Submitted.
Akolekar, D. B., Bhargava, S. K. & Foger, K. (1998). *J. Chem. Soc. Faraday Trans.* **94**, 155–160.
Akolekar, D. B., Chaffee, A. & Howe, R. F. (1997). *Zeolites*, **19**, 359–365.
Bazin, D., Sayers, D., Rehr, J. J. & Mottet, C. (1997). *J. Phys. Chem.* **101**, 5332–5336.

Bellussi, G., Perego, G., Carati, A., Gomaro, U. & Fatore, V. (1988). In *Innovation in Material Science*, edited by P. J. Grobet and W. J. Mortier. Amsterdam: Elsevier.
Benfield, R. E., Grandjean, V., Kroll, M., Pugin, R., Sawitowski, T. & Schmid, G. (2001). *J. Phys. Chem. B*, **105**, 1961–1970.
Bhattacharyya, K. G, Talukdar, A. K., Das, P. & Sivasanker, S. (2003). *J. Mol. Catal. A*, **197**, 255–262.
Brust, M., Walker, M., Bethell, M., Schiffrin, D. & Whyman, R. (1994). *J. Chem. Soc. Chem. Commun.* pp. 801–803.
Chen, X., Huang, L., Ding, G. & Li, Q. (1997). *Catal. Lett.* **44**, 123–128.
Eisenberger, P. & Kincaid, B. M. (1978). *Science*, **200**, 1441–1442.
Ellis, P. J. & Freeman, H. C. (1995). *J. Synchrotron Rad.* **2**, 190–195.
Gorodetskii, V. V. & Drachsel, W. (1999). *Appl. Catal. A*, **188**, 267–275.
Greaves, G. N., Durham, P. J., Diakun, G. & Quinn, P. (1981). *Nature (London)*, **294**, 139–140.
Greegor, R. B. & Lytle, F. W. (1980). *J. Catal.* **63**, 476–483.
Guillemot, D., Polisset-Thfoin, M., Bonnin, D. & Borovkov, V. Y. (1999). *Proceedings of the 12th International Zeolite Conference*, edited by M. M. J. Treacy, B. K. Marcus, M. E. Bisher and J. B. Higgins, p. 2079–2087. Warrendale, PA: Materials Research Society.
Gupta, N. M. & Tripathi, A. K. (1999). *J. Catal.* **187**, 343–347.
Haruta, M. (1997*a*). *Cataly. Surv. Jpn*, **1**, 61–73.
Haruta, M. (1997*b*). *Catal. Today*, **36**, 153–166.
Haruta, M., Kobayashi, T., Sano, H. & Yamada, N. (1987). *Chem. Lett.* pp. 405–409.
Haruta, M., Yamada, N., Kobayashi, T. & Iijima, S. (1989). *J. Catal.* **115**, 301–305.
Jeon, J. Y., Kim, H. Y. & Woo, I. S. (2003). *Appl. Catal. B*, **44**, 311–323.
Kageyama, H., Tsubota, T., Kamijo, N. & Haruta, M. (1993). *Jpn. J. Appl. Phys. Suppl.* **32**, 445–451.
Kladis, C., Bhargava, S. K., Foger, K. & Akolekar, D. B. (2000). *Catal. Today*, **63**, 297–303.
Kobayashi, T., Haruta, M., Tsubota, S. & Sano, H. (1990). *Sens. Actuators B*, **1**, 222–227.
Koningsberger, D. C. & Prins, R. (1988). *X-ray Absorption*, edited by D. C. Koningsberger and R. Prins. New York: John Wiley.
Kresge, C. T., Leonowicz, M. E., Roth, W. J., Vartuli, J. C. & Beck, J. S. (1992). *Nature (London)*, **359**, 710–712.
Rich, A. M., Armstrong, R. S., Ellis, P. J., Freeman, H. C. & Lay, P. A. (1998). *Inorg. Chem.* **37**, 5743–5753.
Ryoo, R., Kim, J. M., Ko, C. H. & Shin, C. H. (1996). *J. Phys. Chem.* **100**, 17718–17721.
Tsubota, S., Haruta, M., Kobayashi, T., Ueda, A. & Nakahara, Y. (1991). *Preparation of Catalysts V*, edited by G. Poncelet, P. A. Jacobs, P. Grange and B. Delmon, p. 695–702. Amsterdam: Elsevier Science.
Uphade, B. S., Yamada, Y., Akita, T., Nakamura, T. & Haruta, M. (2001). *Appl. Catal. A*, **215**, 137–143.
Walker, C. H., St John, J. V. & Neilson, P. W. (2001). *J. Am. Chem. Soc.* **123**, 3846–3847.
Wilson, S. T., Lok, B. M., Messina, C. A., Cannan, T. R. & Flanigen, E. M. (1982). *J. Am. Chem. Soc.* **104**, 1146–1147.
XFIT (1995). *XFIT for Windows 95*. Australian Synchrotron Research Program, Sydney, Australia.
Zhdanov, V. P. & Kasemo, B. (2002). *Surf. Sci. Lett.* **511**, 23–26

 Received 27 August 2003 • Accepted 21 January 2004 